# NMR Solution Structure of a Peptide from the mdm-2 Binding Domain of the p53 Protein that Is Selectively Cytotoxic to Cancer Cells[†,‡]

Ramon Rosal,[§] Matthew R. Pincus,*[,||,⊥] Paul W. Brandt-Rauf,[§] Robert L. Fine,[@] Josef Michl,[⊥] and Hsin Wang[#]

*Department of Environmental Health Sciences, Mailman School of Public Health of Columbia University, 60 Haven Avenue, New York, New York 10032, Department of Pathology and Laboratory Medicine, New York Harbor VA Medical Center, 800 Poly Place, Brooklyn, New York 11209, Department of Pathology, SUNY Downstate Medical Center, 450 Clarkson Avenue, Brooklyn, New York 11203, Experimental Therapeutics Program, Division of Medical Oncology, Columbia University College of Physicians and Surgeons, 650 West 168th Street, New York, New York 10032, and Department of Chemistry, College of Staten Island, 2800 Victory Boulevard, Staten Island, New York 10314*

*Received September 23, 2003; Revised Manuscript Received December 3, 2003*

ABSTRACT: We have recently found that a peptide from the mdm-2 binding domain of the p53 protein induced rapid membranolytic necrosis of a variety of different human cancer cell lines. To determine the role of solution structure in this peptide's selective and rapid tumor membrane disruptive behavior, we have performed two-dimensional NMR on a 32-residue sequence called PNC-27, in both an aqueous cytosolic-like and a mixed organic membrane-mimetic solution environment. In an aqueous milieu, PNC-27 contains three α-helical domains connected by loop structures, forming an S shape, and another similar structure with less helical structure. In a solution environment simulating a membrane, the helical domains found in water increase in length, forming three classes of structures, all of which form a U-shaped helix−coil−helix ensemble. In both solvent systems, this peptide forms amphipathic structures such that its hydrophobic residues coalesce on one face while the polar residues aggregate on the opposite face. The ability to form these unique structures in these two solution environments may allow the PNC-27 peptide to selectively and rapidly disrupt cancer cell membranes.



The p53 protein, which has a critical role in cell cycle control and apoptotic signaling, has been a major target for anticancer therapy since mutated p53 occurs in at least 50% of human cancers (*1*, *2*). Since p53 is catabolized in a process in which it binds to the mdm-2[1] (murine double minute clone 2) to form a complex, whereby its transcriptional activity is blocked through a ubiquitin-dependent proteosome pathway, we devised a strategy for enhancing its activity by designing agents that block formation of this complex (*3*). Since the mdm-2 binding domain of p53 has been identified (*4*), one strategy was to inhibit complex formation using peptides from this mdm-2 binding domain that would compete with p53 for binding to mdm-2. This would result in the stabilization of wild-type p53, overcoming the effects of mutated forms, thus promoting p53-dependent cell cycle arrest and apoptosis in cancer cells (*2*).

Using this strategy, we have found that several peptides from the N-terminal mdm-2 binding domain of p53, viz., residues 12−26, 12−20, and 17−26, linked to a transfer domain of *Drosophila* homeobox protein *Antennapedia* penetratin (KKWKMRRNQFWVKVQRG), called penetratin, on their carboxyl-terminal ends, all induced rapid, nonapoptotic cell death resembling necrosis in many different human and mammalian cell lines, including several cell lines such as SW1417 human colon cancer cells which have the p53 gene homozygously deleted (*3*). None of these peptides, however, was found to have any effect on the growth of nontransformed cells such as BMRPA1 pancreatic acinar cells and on the normal differentiation of cord blood-derived human stem cells into hematopoietic cell lines in the presence of growth factors.

Since the purpose of using these peptides was to block the mdm-2−p53 complex from forming, it was anticipated that they would induce p53-dependent apoptosis. However, we found that they induced rapid cancer cell necrosis rather than apoptosis, and since they are equally cytotoxic to p53 homozygously deleted cell lines, these peptides may be inducing cell death using other mechanisms (*3*). In a recent study, we found that one of these peptides induced necrosis of human breast cancer cell lines with mutant p53 by causing rapid membrane disruption (*5*).

[†] This work was supported in part by NIH RO1 Grant CA 42500, a VA Merit Review Grant, and a grant from the Lustgarten Foundation for Pancreatic Cancer Research to M.R.P. and J.M.; EPA Grants R8825361 and R826685 and NIH RO1 Grant OH007590 to P.W.B.-R.; and NIH RO1 Grant CA 82528 and a Herbert Irving Scholar Award to R.L.F.

[‡] Two sets of atomic coordinates and structure factor files along with $^{1}H$ and $^{13}C$ chemical shift assignments have been deposited in the Protein Data Bank as RCSB entry RCSB019830 and PDB entry 1Q2F and RCSB entry RCSB019833 and PDB entry 1Q2I, respectively.

* To whom correspondence should be addressed. E-mail: matthew.pincus2@med.va.gov.

[§] Mailman School of Public Health of Columbia University.

[||] New York Harbor VA Medical Center.

[⊥] SUNY Downstate Medical Center.

[@] Columbia University College of Physicians and Surgeons.

[#] College of Staten Island.

[1] Abbreviations: CD, circular dichroism; NMR, nuclear magnetic resonance; NOE, nuclear Overhauser effect; CSI, chemical shift index; DQF-COSY, double-quantum-filtered correlation spectroscopy; TOCSY, total correlation spectroscopy; HSQC, heteronuclear single-quantum correlation; DMSO, dimethyl sulfoxide; TMS, tetramethylsilane; DSS, 2,2-dimethyl-2-silapentane-5-sulfonic acid; mdm-2, mouse double minute clone 2; rmsd, root-mean-square deviation.

10.1021/bi035718g CCC: $27.50 
Published on Web 01/30/2004

In designing the three N-terminal p53 peptides, we utilized the X-ray structure of the p53 12−27 peptide bound to an mdm-2 fragment (*4*). In this complex, the p53 peptide adopts a predominantly α-helical structure. The penetratin sequence contains a high percentage of positively charged residues, and since positive charges stabilize the α-helical conformation of peptides if they occur on their carboxyl-terminal ends, we placed the penetratin sequence on the carboxyl-terminal end of the three p53 peptides (*3*). Since these peptides exerted a cytotoxic effect on a variety of different cancer cells that appears to be p53-independent but were designed to adopt a conformation that would bind to mdm-2 competitively with p53, we have been investigating whether these peptides adopt an α-helical conformation in solution and the mechanisms by which they induce preferential cancer cell cytotoxicity.

We have recently shown, using circular dichroism, that the p53 mdm-2 binding domain peptide, corresponding to p53 residues 12−26, linked to penetratin, called PNC-27, contains significant (almost 30%) α-helical structure (*5*). Using time-lapse electron microscopy on breast cancer cells that have been treated for different times with PNC-27, we found that this peptide induces rapid membrane destruction that appears to correlate with its α-helical content (*5*). Because, evidently, its anticancer activity is related to its three-dimensional structure, we have undertaken to determine the three-dimensional structure of this peptide in solution.

In this paper, we report the determined three-dimensional solution structures of the p53 12−26 peptide attached to penetratin, using two-dimensional NMR, in aqueous and nonaqueous (membrane-mimetic) solvents. The use of NMR mixed solvent systems to simulate a membrane environment has been widely used to elucidate protein structures that cannot be attained by X-ray crystallography (*6*, *7*). We further propose a mechanism for our observed cellular effects, based on peptide structure.

## EXPERIMENTAL PROCEDURES

*Peptide*. The p53 12−26 peptide (in bold) attached to penetratin (in italics), **PPLSQETFSDLWKLL***KKWKMRRNQFWVKVQRG*, called PNC-27, was synthesized using solid-phase methods and was purified by HPLC to >95% purity.

*NMR Experiments.* PNC-27 was dissolved at a concentration of 4.0 mM in 10 mM phosphate buffer (pH 5.7) containing 5% DMSO-$d_6$, and in the same concentration in a 4:4:1 $CDCl_3/CD_3OH/H_2O$ low-dielectric mixed solvent system. Samples in the latter solvent system were flame-sealed to ensure the constancy of the solvent composition. NMR experiments were carried out on a four-channel Varian $^{UNITY}$INOVA 600 MHz spectrometer (Varian Inc., Palo Alto, CA) equipped with a triple-resonance probe and *z*-axis pulsed field gradients. Experiments were carried out between 10 and 37 °C. Only the 37 °C results are presented here. Proton assignments were accomplished with TOCSY (mixing time of 70 ms), NOESY (mixing times of 100 and 300 ms), and DQF-COSY experiments (*8*). These homonuclear data sets were acquired with 2048 and 400 complex points in $t_2$ and $t_1$, respectively. Typically, data were scanned 16 times with a sweep width of 8000 Hz in both $^1$H dimensions. Relaxation delays of 1.5 and 2 s were used for experiments in the aqueous solution and in the mixed solvent system, respectively.

The assignments were assisted and confirmed by natural abundance $^{13}$C−$^1$H HSQC and $^{13}$C HSQC-TOCSY. Conventional phase cycling was used instead of gradient selection to avoid sensitivity loss. These heteronuclear data sets were acquired with 1024 and 512 complex points, and sweep widths of 8000 and 20 000 Hz, in $t_2$ ($^1$H) and $t_1$ ($^{13}$C), respectively. Typically, a relaxation delay of 1.2 s was used with 64 and 128 scans for HSQC and HSQC-TOCSY, respectively. The WET scheme was used to suppress the water signal (*9*) in all experiments.

The deuterium solvent lock was 5% DMSO-$d_6$ for the aqueous solution and $CD_3OH$ for the mixed solvent system. The chemical shift references are made as follows. DSS was used in the 5% DMSO-$d_6$ aqueous solution to reference both $^1$H and $^{13}$C shifts. The $^{13}$C/$^1$H referencing ratio Ξ is determined to be 0.251 449 60. On the other hand, TMS is used in the mixed solvent system to reference $^1$H and $^{13}$C shifts with the Ξ ratio determined to be 0.251 450 06. These Ξ ratios are very similar to published values of 0.251 449 52 and 0.251 450 02 for DSS and TMS, respectively (*10*).

NMR data were processed with NMRPIPE (*11*) and analyzed with NMRVIEW (*12*). Proton and proton-associated carbon assignments (including aromatic groups) were complete except for some lysine side chain at $\gamma-\epsilon$ positions (Tables 1 and 2 of the Supporting Information). Unique NOE distance constraints (480 from the aqueous solvent and 364 from the nonaqueous solvent) were calibrated with the medium intensity at 2.7 Å. Two hundred structures each were calculated for each solvent system using DYANA (*13*), and the 20−30 best structures were selected for display. Computer rendering of NMR structures was done using Molmol (*14*) and DS Viewer Pro 5 (Accelrys Inc., San Diego, CA).

## RESULTS

*NOESY Results*. Figures 1 and 2 show the NH−HA and NH−NH NOESY spectra, respectively, for PNC-27 in aqueous solvent (left panels) and in nonaqueous solvent (4:4:1 chloroform/methanol/water mixture) (right panels). The residue assignments were largely based on the traditional two-dimensional $^1$H−$^1$H approach augmented by identification through the use of $^1$H−$^{13}$C heteronuclear spectroscopies. The latter approach removes all ambiguity in the side chain proton assignments. Both Figures 1 and 2 show that there are many cross-peaks in both solvents, almost all of which range from short-range ($i-i+2$) to intermediate-range ($i-i+4$) interactions. Importantly, there are many such peaks in the aqueous solvent (Figures 1 and 2, left panels), indicating significant structure.

Figure 3 shows plots of the distance constraint distribution versus interresidue distance for the peptide in aqueous (left) and nonaqueous (right) solvents. It can be seen that the majority of the constraints are either intraresidual or sequential. In the nonaqueous system, there appears to be more $i-i+3$ and $i-i+4$ interactions. Figure 4 shows that these interactions exist in extended regions throughout much of the molecule in the nonaqueous solution, as compared with a short middle section in the aqueous solution. Interestingly, the $d_{\alpha N}(i,i+2)$ interactions, which may be indicative of the

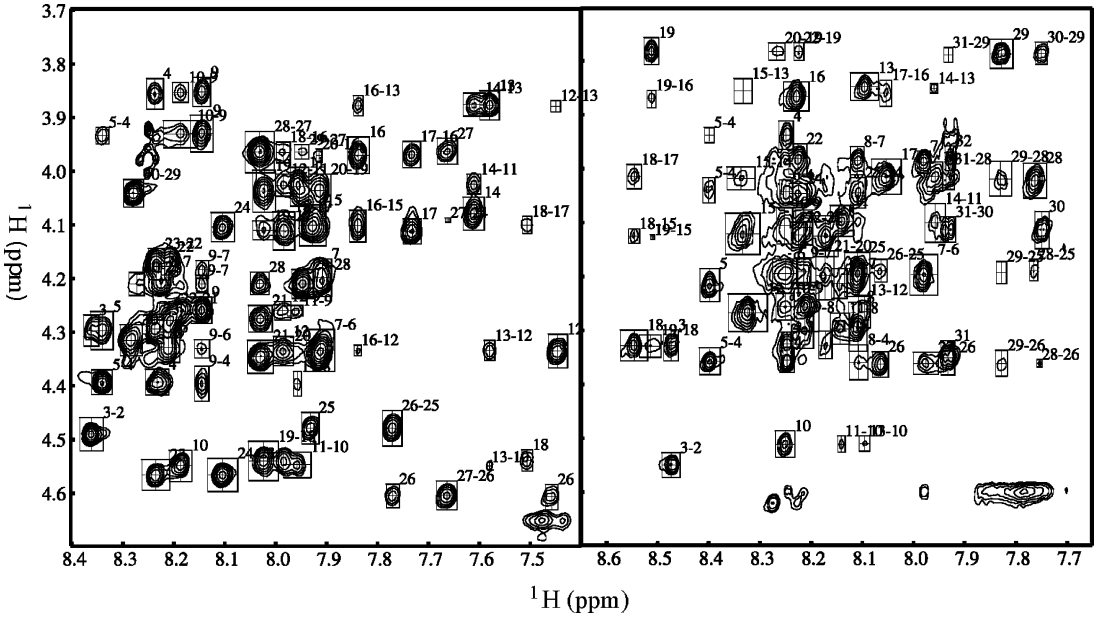


FIGURE 1: NOESY fingerprint region spectra of PNC-27 in aqueous medium [5% DMSO-$d_6$ in 10 mM phosphate buffer (pH 5.7)] (left) and in nonaqueous medium (4:4:1 $CDCl_3$/MeOH/$H_2O$ mixture) (right). Interacting protons are identified in both panels.

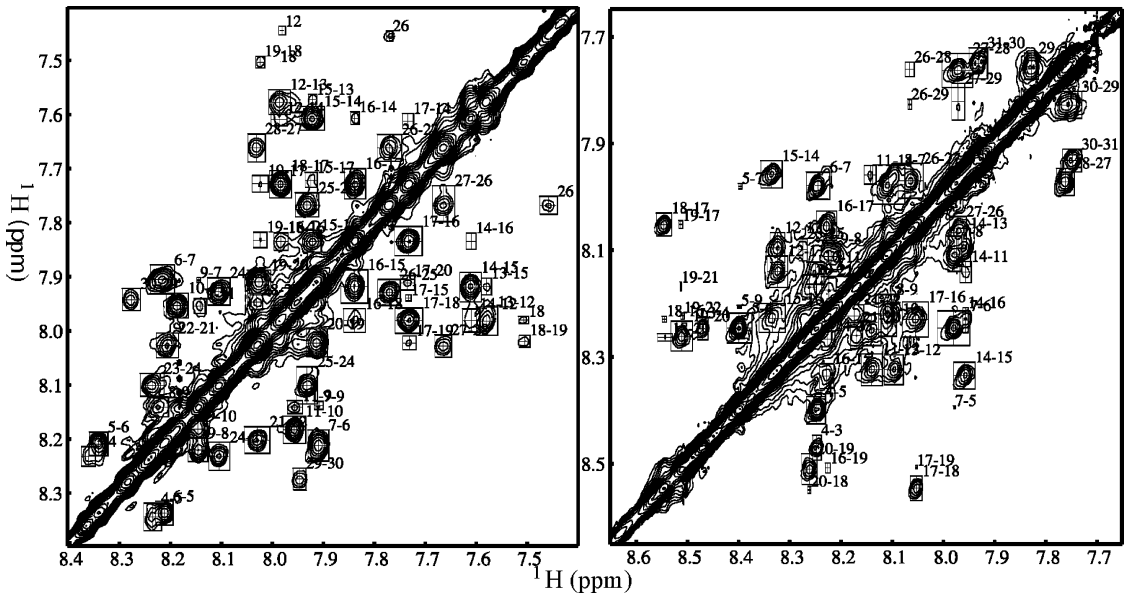


FIGURE 2: NOESY (NH−NH) regions of PNC-27 in aqueous (left) and nonaqueous (right) solvents. Interacting residue protons are identified in both panels.

shorter $3_{10}$-helix or turns, are more prevalent in the aqueous solution. Thus, it can be deduced that the mixed solvent favors structures such as α-helices, whereas in the aqueous solution, the helical pitch would be shorter and is more characteristic of $3_{10}$-helices. It can also be seen that the N-terminus ($i < 5$) is relatively unstructured in both solvents and that the medium- to long-range NOEs are more prevalent in the penetratin segment of the peptide (residues 16−32) in the nonaqueous solution.

*Secondary Structure Propensity Predicted by the Chemical Shift Index (CSI).* Although PNC-27 is a sizable peptide and a proposal was made that the C-terminal penetratin segment might induce the formation of helical structure (*3*), it was initially anticipated that the peptide might not display a well-defined structure in aqueous solution. On the other hand, chemical shifts, particularly those of carbons, are known to be indicative of secondary structure (*15*, *16*). Thus, the design of our NMR experiments included $^{13}C-^1H$ heteronuclear techniques that will not only confirm assignments but also shed light on the propensity of secondary structure.

The CSI prediction of secondary elements was computed with a tcl script in the NMRVIEW program (*12*). The script makes adjustments with regard to the reference standards (DSS or TMS) as well as pH and temperature. However, no known adjustments can be made for the modification of solvent composition, such as 5% DMSO-$d_6$ or the mixed organic/water system. As shown in panels A and B of Figure 5, PNC-27 in the 5% DMSO-$d_6$ aqueous solution exhibits a high helical propensity between residues 11 and 28 with an interruption at residues 22 and 23. The prediction is made with two of the most commonly used CSI databases (*15*) (*16*) and is consistent with the result of structure calculation (see below). The strength of the CSI structure prediction method relied almost exclusively on the HN and HA

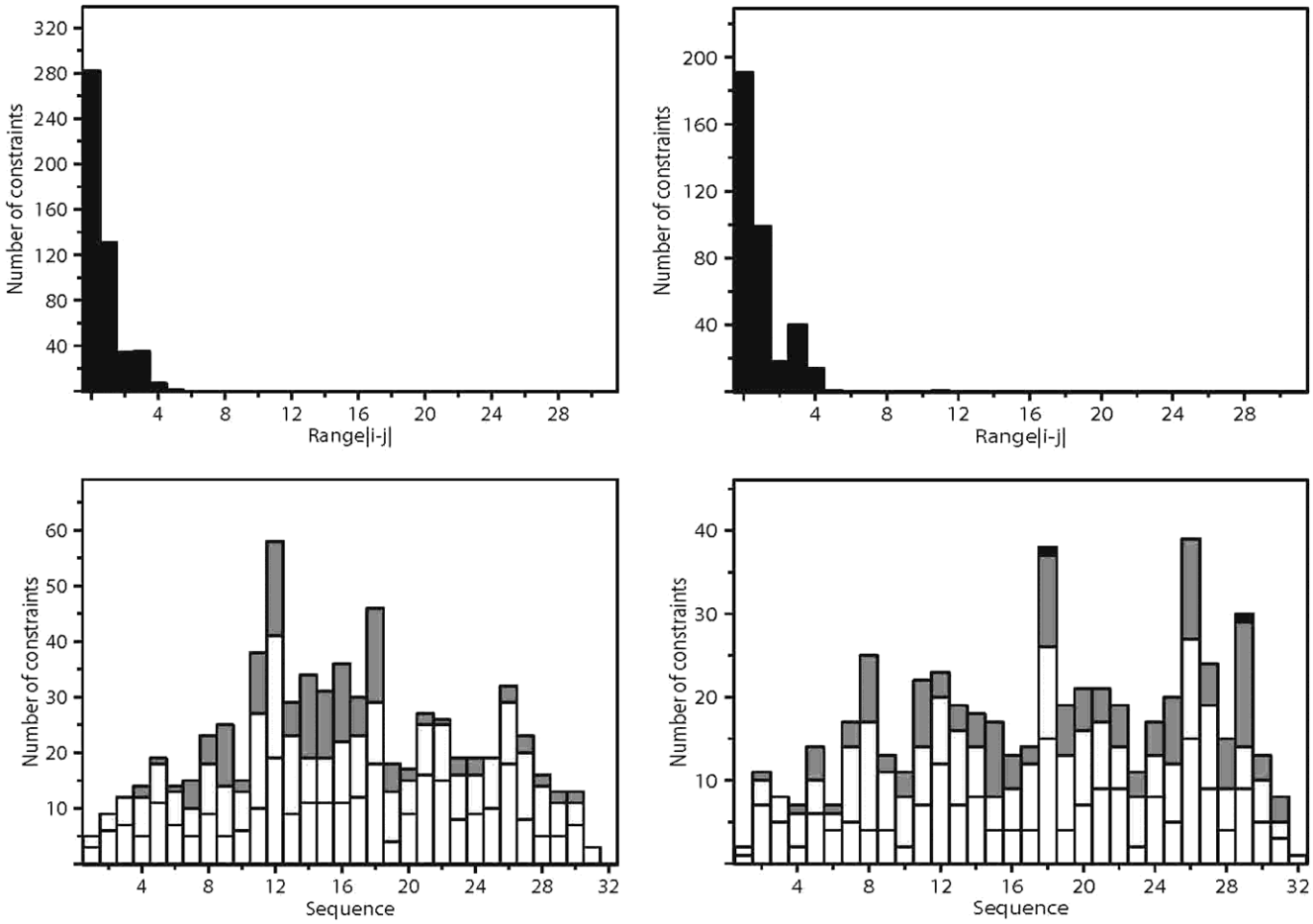


FIGURE 3: NOE constraint distribution for PNC-27 (top) in aqueous (left) and nonaqueous (right) solvents as a function of the interresidue distance and NOE constraints at each location (right): intraresidue (white), sequential (light gray), short- and intermediate-range ($i-i+2$, $i-i+3$, and $i-i+4$) (dark gray), and long-range ($i-i+5$ and greater) (black) interactions from the NOE experiments for PNC-27 in aqueous (left) and nonaqueous (right) solvents.

assignments, because predictions based on Cα and C$\beta$ largely canceled each other out.

The CSI does not predict reliably the secondary structure elements of PNC-27 in the membrane-mimetic system. Using the random coil database from Wishart *et al*. (*15*), PNC-27 is predicted to be almost void of any structures (Figure 5C). On the other hand, with Richarz and Wüthrich (*16*), a predominantly α-helical structure is predicted (Figure 5D). The latter prediction turns out to be correct. Inspection of Tables 1 and 2 of the Supporting Information indicates a general upfield shift in the carbon assignments in the mixed solvent relative to the aqueous solution. This can be largely ascribed to a difference of 2−3 ppm when DSS is used instead of TMS as reference standard (*15*). It is likely that the modification of solvent composition adds a further variable that makes prediction based on carbon shifts less reliable. One should also note that although carbon shifts have proven to be very reliable in predicting secondary structures in proteins, their use in peptide structures has not been adequately tested because they are less readily available than proton shifts.

*Peptide Structures in the Aqueous Solvent*. In the aqueous solvent, PNC-27 contains several helical domains that are connected by coiled structures, which differ considerably from one another (overall rmsd of 5−6 Å). This is primarily due to the diminished number of the medium- to long-range NOE constraints in the penetratin segment. The mean rms deviations among the 20 structures decrease to 0.98 ± 0.52 Å for backbone and 1.70 ± 0.61 Å for heavy atoms if only the more ordered segment (residues 7−20) is considered.

As shown in Figure 6A, most structures, called class I structures, in aqueous solvent were found to have an S shape with α-helices occurring between residues 7 and 11, 16 and 19, and 24 and 28. As can also be seen in Figure 6A, residues 12−15 form a loop in these structures. A one-turn α-helix can also be fit to the NOE data for residues 12−15, resulting in one helix between residues 7 and 19, as shown in Figure 6B. In structures containing this longer helix, called class II structures, given the nonhelical NOE constraints for residues 20−23, which form loops, it is not possible to fit an α-helix to residues 24−28, which then form three consecutive turns, as also shown in this figure.

In the class I structures (Figure 6A), continguous helical domains form at right angles to one another. In class II structures, the single helical domain forms a right angle to the loop structures adopted by the penetratin domain on its carboxyl-terminal end.

Importantly, residues 7−12 and 12−15 correspond to residues 18−26 of p53 which are in the segment directly involved in the binding of p53 to mdm-2 (*4*). In all structures, residues 7−11 (residues 18−22 in p53, respectively) adopt an α-helical conformation, and in class II structures, residues 7−19 (that includes residues 18−26 of p53) adopt this conformation. In the X-ray structure of p53, residues

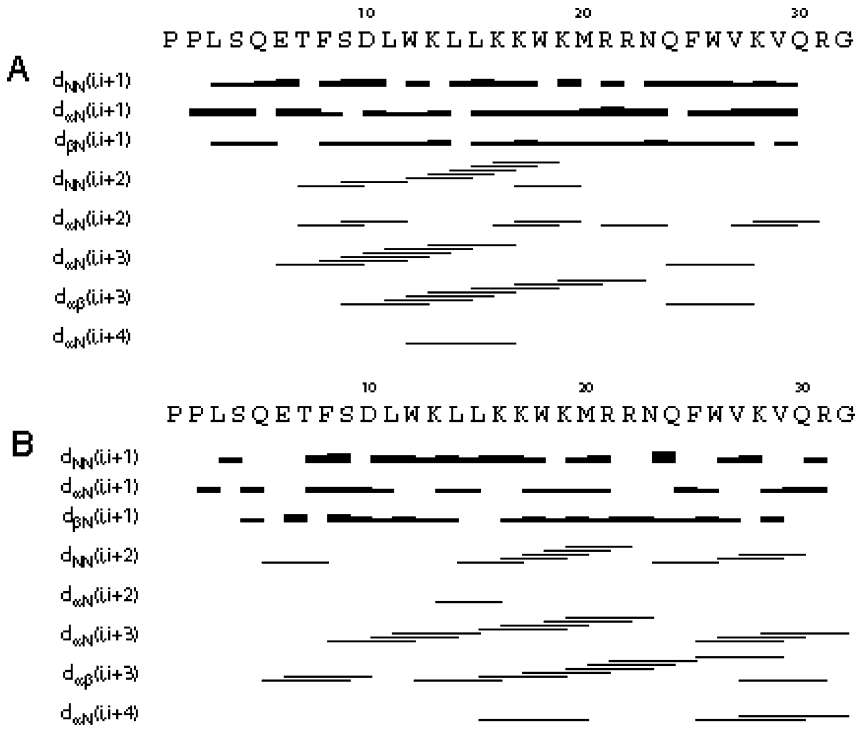


FIGURE 4: NOE connectivity diagrams for PNC-27 in aqueous (A) and nonaqueous solutions (B).

19−26 occur in an α-helix when bound to mdm-2 (*4*). Thus, in an aqueous solution, this domain appears to adopt structures in the unbound state that are similar to the one that occurs when it is bound to mdm-2.

*Helical Content*. Since the number of residues in an α-helical conformation is almost the same for each of the structures that satisfied the NOE constraints, despite conformational differences among them, we compute that the helical content of this peptide in aqueous solvent is 38%, which is higher than the value of 27% from CD measurements (*5*) and lower than the value of 50% computed for this peptide using an Ising model that includes the effects of charges in water. This comparison is limited, however, by the assumption that all structures that fit the NOE constraints contribute equally to an ensemble average. In any case, it is clear that the peptide in the aqueous solution contains significant helical structure.

*Peptide Structures in the Nonaqueous Solvent*. In the nonaqueous solvent, many structures also fit the NOE constraints but were significantly more similar to one another, the overall backbone and all-atom rms deviations being 1.0 and 1.2 Å, respectively. These structures contained more α-helical domains that those found in the aqueous solvent. We found that we could classify all of the structures satisfying the NOE distance constraints into three types of structures: class I, as shown in Figure 7A, with α-helices from residues 7−14, two reverse turns at residues 15−17, and α-helices at residues 18−22 and 24−31; class II, as shown in Figure 7B, with two reverse turns from residues 7−9 and with α-helices from residues 10−14, 18−22, and 24−31; and class III, as shown in Figure 7C, with α-helices from residues 7−22 and 24−31.

The average helical content for this peptide in the nonaqueous solvent is 65% (for class I and II structures) and 75% for class III structures, a significant increase compared with that of the peptide in the aqueous solvent (under the assumption that all structures contribute equally to the ensemble average). This difference in helical content is due to extension of the helical segment from residues 7−12 in the aqueous solvent to residues 7−14 or 7−22 (class I and III structures, respectively) in the nonaqueous solvent and from residues 24−28 in a subset of the structures in the aqueous solvent to residues 24−31 in all of the structures in the nonaqueous solvent. In the nonaqueous medium, the penetratin segment (residues 18−32) has more α-helical structure since residues 24−31 are α-helical in all of the structures, while in the aqueous solvent, only two residues, 18 and 19, occur in the α-state in class II structures (Figure 4B) and, additionally, in class I structures, residues 24−28 (Figure 4A).

*Recurrent Structural Motifs in Aqueous and Nonaqueous Media*. Despite conformational differences among the structural classes in each solvent and differences in structures for the peptide in the two different solvents, there appear to be recurring common structural motifs. As noted for the structures in panels A and B of Figure 6 in the aqueous solvent, all of the structures in the nonaqueous solvent shown in panels A−C of Figure 7 have two mainly helical domains that occur at roughly right angles to one another; these two domains are separated by loops in the structures at either residues 16 and 17 (Figure 7A,B) or 23 and 24 (Figure 7C), forming a bent U-shaped helix−loop−helix structure. As noted above, for the structures in the aqueous solvent (Figure 6A,B), these loops occur at residues 12−15 and 21−23 in class I structures while they occur at residues 20 and 21 in class II structures.

Importantly, the p53 peptide segment of residues 1−15 (p53 residues 12−26, respectively) and penetratin Lys16 and Lys17 form amphipathic structures, irrespective of differences in the lengths of helices or of the conformations of intervening loops. This is shown in Figure 8, in which a representative space filling structure of the class III non-

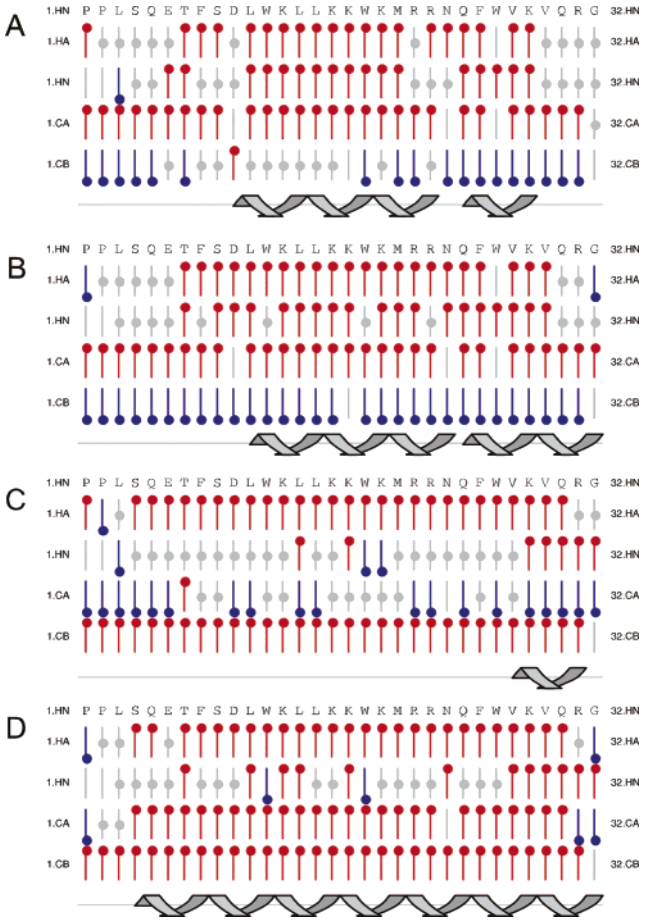


FIGURE 5: Secondary structure propensity predicted by the chemical shift index (CSI). Panels A and B are predicted for PNC-27 in the aqueous solution and panels C and D in the 4:4:1 chloroform/methanol/$H_2O$ mixture. The random coil chemical shift database of Wishart *et al*. (*15*) is used in panels A and C, and that of Richarz and Wüthrich (*16*) is used for panels B and D. The plots were made such that the propensity for helix is designated as +1 (shown in red) and that for sheet as −1 (shown in blue). Chemical shifts within the tolerance range of random coil are designated as 0 (shown in gray). The plots were made with NMRVIEW.

aqueous conformations is shown. Essentially identical results were obtained for the other classes of structures in both solvent systems (not shown).

This view shows that the peptide has a hydrophobic face involving two clusters shown as green-colored residues. In one cluster, Pro1, Pro2, and Leu3 form one domain, and on the same face, Leu11, Trp12, Leu14, and Leu15 (the Phe8 side chain also points toward this hydrophobic surface) form a second hydrophobic domain. Hydrophilic residues protrude from the opposite face such that they form two subdomains: one that involves negatively charged or neutral hydrophilic residues, shown in red in Figure 6, including Ser4, Gln5, Glu6, Ser9, and Asp10; and another that involves positively charged residues, shown in dark blue, i.e., Lys13, Lys16, and Lys17. The penetratin domain shows more complex patterns that differ from structure to structure. However, in all classes of structures, certain polar residues form discrete hydrophilic domains: Lys19 (blue), Asn23 and Asn24 (red), and Lys28 and Arg31 (blue). Since the amphipathic distribution of residues is common to all structures, it may point to a functional role for this peptide, as discussed in the next section.

## DISCUSSION

*PNC-27 Is a Membrane-Active Peptide*. This study of the solution NMR structure of the mdm-2 binding p53 12−26 peptide, attached to penetratin, was prompted by our findings that it is selectively cytotoxic to several types of cancer cells and that this cytotoxicity, which results from it being membrane-active, appears to correlate with its structure when it is membrane-bound (*3*, *5*). The existing X-ray structure for p53 omits this domain (*17*) and the transactivating domain (residues 1−92) within which it occurs. Although there is an X-ray structure of the mdm-2 binding domain of p53 (residues 12−27) bound to an mdm-2 fragment (*4*), at least part of the p53 12−26−penetratin peptide activity appears to be independent of p53-induced mechanisms. Furthermore, no X-ray or NMR structure exists for the 12−26 peptide attached to penetratin. We therefore elected to investigate whether the full peptide attached to the leader sequence on its carboxyl-terminal end has any well-defined three-dimensional structure especially in a membrane-like, i.e., low-dielectric, environment.

*PNC-27 Partially Folds in Water*. Unlike a number of peptides in the aqueous solution, this peptide contains significant structure from the NOE data (Figures 1 and 2). In class I structures, three helical segments occur, at residues 7−11, 12−15, and 16−19, and in class II structures, one long helix forms from residues 7−19. In both classes, there are distinct domains that form right angles to one another, especially in the class I S-shaped structures in which helical domains occur at right angles to one another.

*PNC-27 Is Highly Structured in a Nonaqueous, Membrane-Mimetic Solvent*. In the nonaqueous solvent, the peptide also adopts structures that can be placed in three classes that are similar to the ones obtained in the aqueous solvent, except that the helical domains are extended by several residues and α-helices occur that include residues 12−15 and 24−28 simultaneously as noted in the above paragraph and in the Results. However, in contradistinction to the classes of structures for the peptide in the aqueous solvent, every class of structures for the peptide in the nonaqueous solvent has two helices that are oriented at roughly right angles to one another, forming a bent helix−loop−helix motif, resembling a U-shaped rod.

*Possible Conformational Transition Pathway*. As noted above, class I structures in the aqueous solvent (Figure 6A) have two sets of α-helices at right angles to one another: residues 7−11 and 15−19, separated by a loop of residues 12−14; and residues 15−19 and 24−28, separated by a loop of residues 20−23. If the first α-helix is extended from residue 7 to 19, and the third helix is extended from residue 24 to 30, the resulting structure strongly resembles the class III structures in the nonaqueous solvent where the helix from residue 7 to 19 (22 in the class III structures) is at right angles to the one from residue 24 to 28 (30 in the class III structures). Alternatively, in the aqueous class I structures, if the loop structures of residues 20−23 are rotated so that they are in line with the helix of residues 15−19, then the helices of residues 7−12 are at right angles to the helices at residues 15−19 and 24−28, in a structure resembling class I and II structures in the nonaqueous solvent. From these considerations, it appears to be plausible that the aqueous class I structures may be the "predecessors" of the structures

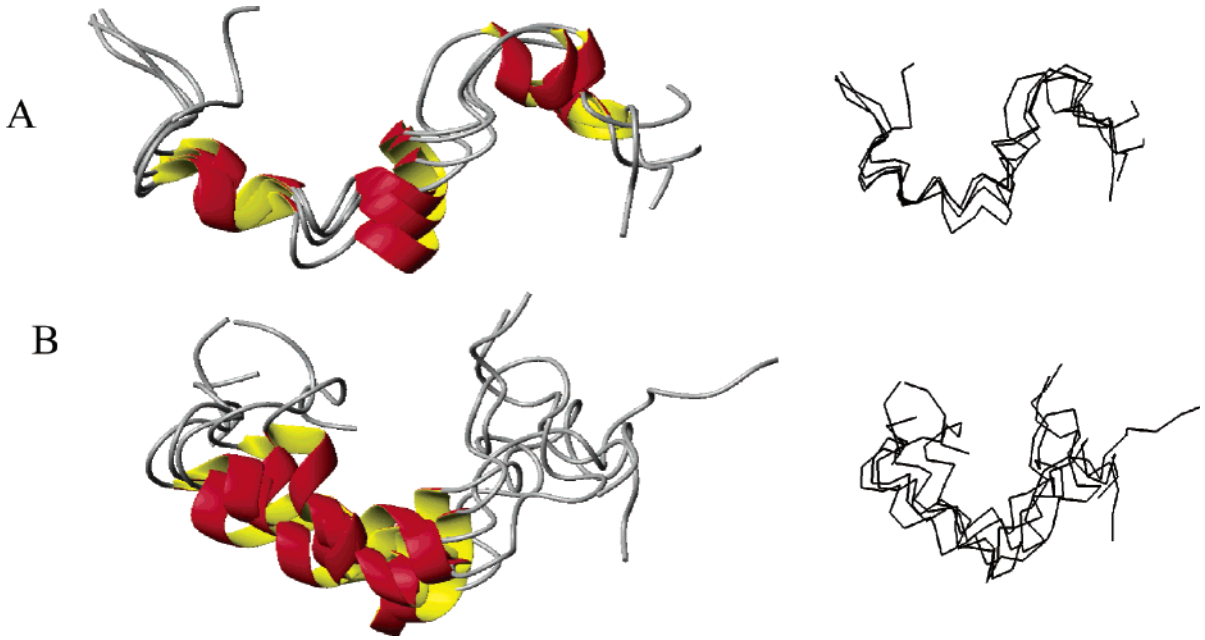


FIGURE 6: Solid ribbon figures of the two classes (A and B) of structures that fit the NOE constraints for PNC-27 in the aqueous solvent. Helical segments are shown as wide colored ribbons. Residue labels are shown along the backbone. Included with each ribbon structure is a Cα trace of the depicted structures.

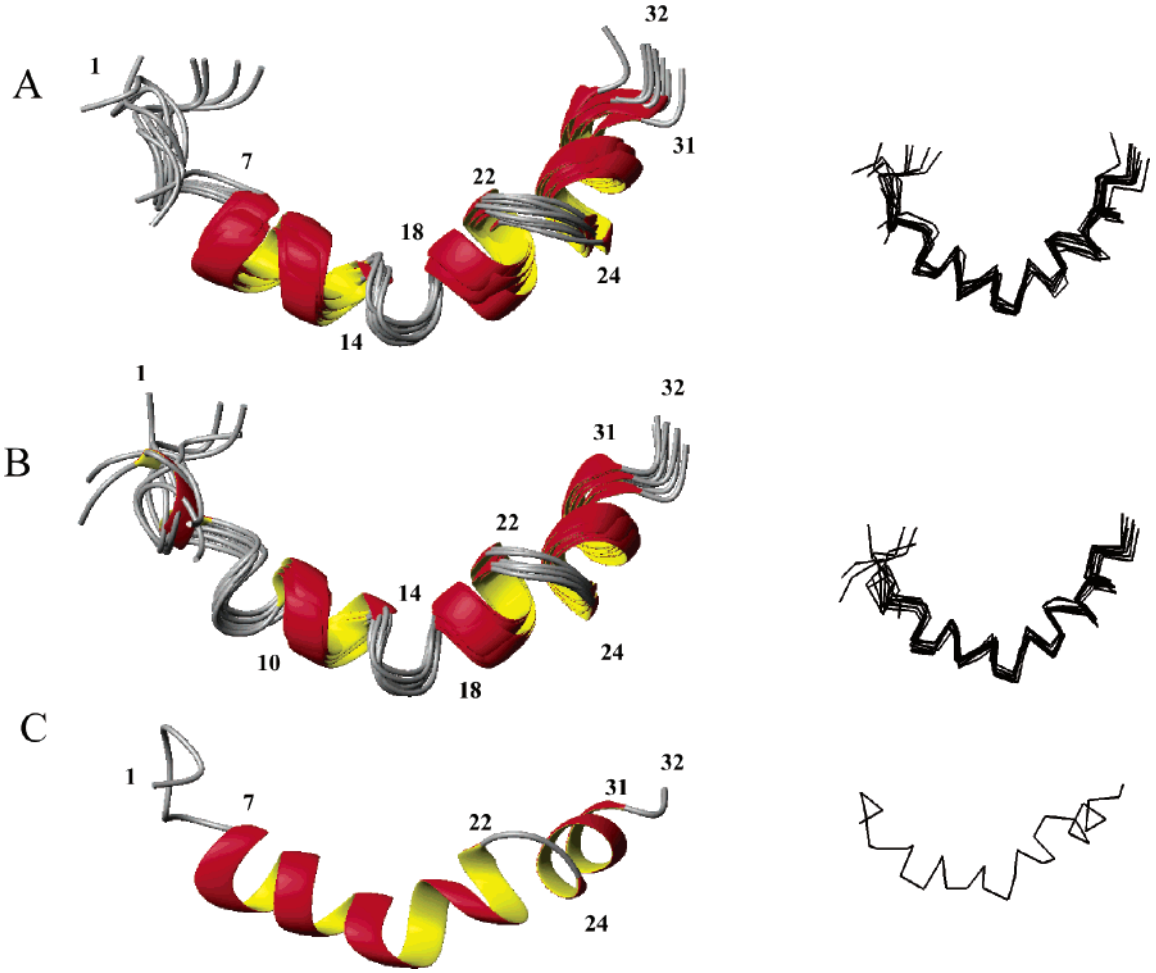


FIGURE 7: Solid ribbon figures of the three classes (A−C) of structures that fit the NOE constraints for PNC-27 in the nonaqueous solvent. Helical segments are shown as wide colored ribbons. Residue labels are shown along the backbone. Included with each ribbon structure is a Cα trace of the depicted structures.

found in the nonaqueous medium that form well-defined helix−loop−helix structures.

*Functional Significance of Amphipathic Helix−Loop−Helix Structures*. This structural motif has been observed in

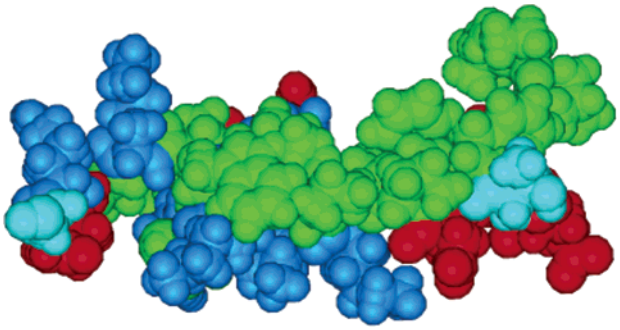

FIGURE 8: Space filling model showing amphipathic structure formation in PNC-27 for a class III structure that satisfied the NOE constraints in the nonaqueous solvent. The color scheme is as follows: green for hydrophobic domains, red for hydrophilic, neutral, or negatively charged residues, and blue for positively charged residues. The amino terminus is at the left, while the carboxyl terminus is at the right. The pattern was identical for the class I S-shaped aqueous structures (not shown).

a number of peptides, containing 20−30 amino acid residues, that adopt helix−loop−helix structures and that are known to be membrane-active, including melittin, the active component of bee venom that induces disruption of red cell membranes (*18*) and the antimicrobial peptide that causes lysis of bacterial membranes, magainin (*19*).

A cardinal feature of this structural motif for these peptides is its amphipathic nature. Clustering of hydrophobic groups on one face of the structures and hydrophilic groups on the opposite face allows these peptides to become membrane-active. For PNC-27, the hydrophobic groups cluster on one face of the molecule while the hydrophilic groups cluster on the opposite face and further segregate into positively and negatively charged domains as shown in Figure 8. Unlike melittin, which is unstructured in water (*9*), PNC-27 adopts amphipathic structures in an aqueous environment. This feature would allow it to act rapidly on tumor cell membranes. In the extracellular matrix, the precursor S-shaped aqueous form (Figure 6A) would intercalate in the cell membrane and, being amphipathic, would be membrane-active. It would further undergo relatively small conformational rearrangements to adopt the full U-shaped helix−loop−helix structure.

In addition to being membrane-active as amphipathic forms, U-shaped helix−loop−helix structures have been observed to form toroidal pores within the membrane, thereby further promoting membrane lysis (*20*, *21*). This conformational feature for PNC-27 in the membrane-like solvent may promote formation of such pores, further conferring on it membranolytic activity. The PNC-27 peptide, which from our electron microscopy studies appears to rapidly lyse the membranes of cancer cells through uniform pore formation (*5*), may do so as a result of these unique solution structures.

## ACKNOWLEDGMENT

The CSI NMR instruments were funded by the National Science Foundation (Grant BIR-9214560), and the facility is operated by the CUNY Center for Applied Biomedicine and Biotechnology and the College of Staten Island.

## SUPPORTING INFORMATION AVAILABLE

Proton and carbon assignments for PNC-27. This material is available free of charge via the Internet at http://pubs.acs.org.

## REFERENCES

1. Levine, A. J. (1997) *Cell 88*, 323−331.
2. Prives, C., and Hall, P. A. (1999) *J. Pathol. 187*, 112−126.
3. Kanovsky, M., Raffo, A., Drew, L., Rosal, R., Do, T., Friedman, F. K., Rubinstein, P., Visser, J., Robinson, R., Brandt-Rauf, P. W., Michl, J., Fine, R. L., and Pincus, M. R. (2001) *Proc. Natl. Acad. Sci. U.S.A. 98*, 12438−12443.
4. Kussie, P. H., Gorina, S., Marechal, V., Elenbaas, B., Moreau, J., Levine, A. J., and Pavletich, N. P. (1996) *Science 274*, 948−953.
5. Do, T. N., Rosal, R. V., Drew, L., Raffo, A. J., Michl, J., Pincus, M. R., Friedman, F. K., Petrylak, D. P., Cassai, N., Szmulewicz, J., Sidhu, G., Fine, R. L., and Brandt-Rauf, P. W. (2003) *Oncogene 22*, 1431−1444.
6. Girvin, M. E., Rastogi, V. K., Abildgaard, F., Markley, J. L., and Fillingame, R. H. (1998) *Biochemistry 37*, 8817−8824.
7. Girvin, M. E., and Fillingame, R. H. (1993) *Biochemistry 32*, 12167−12177.
8. Wuthrich, K. (1986) *NMR of proteins and nucleic acids*, Wiley, New York.
9. Smallcombe, S. H., Patt, S. L., and Keifer, P. A. (1995) *J. Magn. Reson., Ser. A 117*, 295−303.
10. Cavanagh, J., Fairbrother, W. J., Palmer, A. G., and Skelton, N. J. (1996) *Protein NMR Spectroscopy: Principle and Practice*, Academic Press, San Diego.
11. Delaglio, F., Grzesiek, S., Vuister, G. W., Zhu, G., Pfeifer, J., and Bax, A. (1995) *J. Biomol. NMR 6*, 277−293.
12. Johnson, B. A., and Blevins, R. A. (1994) *J. Biomol. NMR 4*, 603−614.
13. Guntert, P., Mumenthaler, C., and Wutrich, K. J. (1997) *J. Mol. Biol. 273*, 283−298.
14. Koradi, R., Billeter, M., and Wüthrich, K. (1996) *J. Mol. Graphics 14*, 51−55.
15. Wishart, D. S., Bigam, C. G., Holm, A., Hodges, R. S., and Sykes, B. D. (1995) *J. Biomol. NMR 5*, 67−81.
16. Richarz, R., and Wüthrich, K. (1978) *Biopolymers 17*, 2133−2141.
17. Cho, Y., Gorina, S., Jeffrey, P. D., and Pavletich, N. P. (1994) *Science 265*, 346−355.
18. Pincus, M. R. (2001) *The Physiological Structure and Function of Proteins*, 3rd ed., Academic Press, New York.
19. Dathe, M., and Wieprecht, T. (1999) *Biochim. Biophys. Acta 1462*, 71−87.
20. Hallock, K. J., Lee, D.-K., and Ramamoorthy, A. (2003) *Biophys. J. 84*, 3052−3060.
21. Naito, A., Nagao, T., Norisada, K., Mizuno, T., Tuzi, S., and Saito, H. (2000) *Biophys. J. 78*, 2405−2417.

BI035718G